

In-vitro investigation of the relationship between microvascular structure and ultrasound contrast agent dynamics

Peiran Chen¹, Simona Turco¹, Ruud J.G. van Sloun¹, Andreas Pollet², Jaap den Toonder², Hessel Wijkstra^{1,3}, Massimo Mischi¹

¹ Dept. Electrical Engineering, Eindhoven University of Technology, Eindhoven, Netherlands

² Dept. Mechanical Engineering, Eindhoven University of Technology, Eindhoven, Netherlands

³ Dept. Urology, Amsterdam University Medical Centers, Amsterdam, Netherlands

Email: P.Chen1@tue.nl

Abstract—Prostate cancer (PCa) is the second leading cause of cancer mortality in men in western countries. Tumor-driven angiogenesis is a recognized hallmark of cancer. Typical features of angiogenic vasculature include increased microvascular density (MVD), smaller vessel diameter and higher tortuosity, resulting in complex blood-flow patterns. Dynamic contrast-enhanced ultrasound (DCE-US) widely provides a noninvasive diagnostic tool for PCa detection with the passage of ultrasound contrast agents (UCAs) through the prostate. Analysis of the UCA dispersion kinetics in the tumor vasculature has shown promise for PCa diagnostics, but a clear link between the estimated kinetics parameters and the underlying microvascular structure is still lacking. In this work, modeling the prostate microvasculature as a porous medium, we developed tissue-mimicking phantoms with variable pore size, representing different MVD and vessel diameter. The UCA flow through the phantoms was recorded by DCE-US, and UCA velocity and dispersion coefficient were estimated by model-based deconvolution. In general, phantoms reproducing increased MVD and smaller vessel diameter lead to increased velocity and decreased dispersion coefficient. This is line with our in-vivo findings in PCa patients. Further validation will be performed by in-silico simulation and more complex in-vitro phantoms in the future.

Index Terms—prostate cancer, dynamic contrast-enhanced ultrasound, flow dynamics, tumor-driven angiogenic microvasculature, porous media phantoms

I. INTRODUCTION

Prostate cancer is the most frequently diagnosed cancer in men in western countries [1]. In clinical routine, the golden standard for prostate cancer diagnosis is the 12-core transrectal ultrasound-guided systematic biopsies, uniformly sampled on the prostate. However, biopsies suffer from the overdiagnosis of insignificant prostate cancer and underdiagnosis of significant cancer [2, 3]. Moreover, biopsies are invasive, painful and carry a high risk of infection.

As a noninvasive diagnostic tool, transrectal dynamic contrast-enhanced ultrasound (DCE-US) allows real-time analysis of vasculature of the prostate by imaging the blood flow with the help of intravenously injected ultrasound contrast agents (UCAs). Thanks to the UCA's size of 1-10 μm , which is similar to the size of red blood cells, UCAs can flow through the entire microvasculature network.

Of particular interest is neo-angiogenesis associated with tumor growth. Tumor-driven angiogenesis is a recognized hallmark of cancer. Angiogenic microvasculature is characterized by increased microvascular density (MVD), smaller vessel diameter and high tortuosity. This irregular and chaotic network results in complex blood-flow patterns [4, 5]. Analysis of time-intensity curves (TICs) obtained from DCE-US loops enables assessment of blood flow. TICs are measured by collecting pixel intensity changes over time at a specific pixel point in the DCE-US loops, representing the UCA concentration temporal evolution. By performing semi-quantitative analysis of TICs, perfusion-related parameters such as peak intensity, wash-in time and mean transit time could be extracted. The differences of these parameters between benign and tumor tissue have been exploited by several researchers to assess tumor perfusion [6, 7, 8]. However, tissue perfusion quantification is strongly affected by ultrasound scanner settings and the complex physiological conditions in organs, leading to unreliable tumor detection [9, 10].

Alternatively, tumor detection by analysis of the UCA dispersion kinetics in microvasculature has shown promise for prostate cancer diagnostics [11, 12, 13, 14]. Considering the UCA concentration evolution over time as the result of a convective dispersion process, the mono-dimensional convective-dispersion equation is employed to model this process. The modified local density random walk model has been proposed as a solution of this equation in the time domain, providing assessment of the microvascular architecture by estimation of a local dispersion parameter, κ , given by the ratio of squared velocity over dispersion coefficient. In prostate cancer, higher values of κ , which means relatively low dispersion with respect to convection, have been shown to correlate with the presence of malignant tissue [11]. More recently, considering the microvasculature as a dynamic system, van Sloun *et al.* proposed a method to locally identify the impulse response of the system by input-output analysis of TICs, enabling separate estimation of velocity and dispersion coefficient. In line with previous studies in the prostate, increased velocity and decreased dispersion were observed in tumor tissue [12].

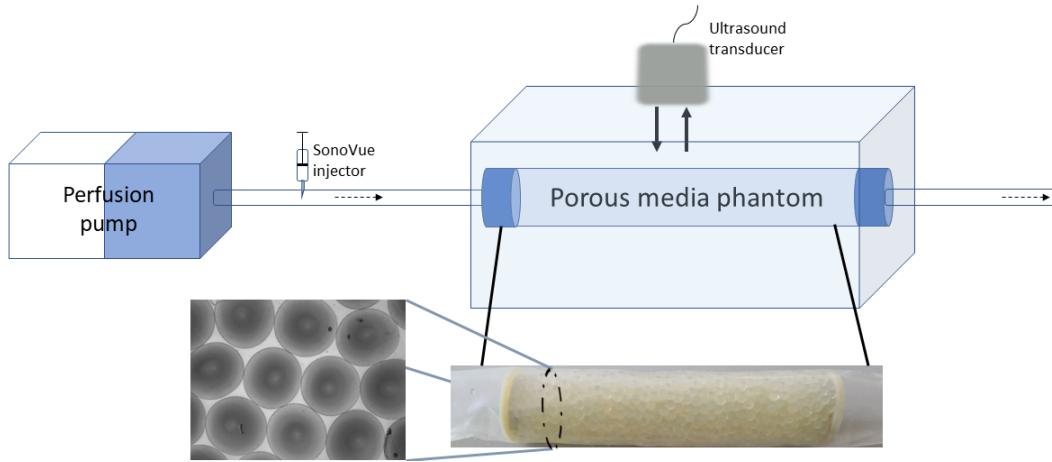


Fig. 1. Schematic overview of the in-vitro set-up.

Despite this, a clear link between the estimated parameters and the underlying microvascular structure is still lacking.

In response, in this work, we developed an in-vitro experimental set-up including dedicated tissue-mimicking phantoms to investigate this relationship. By taking a macroscopic view of the prostate microvascular network, UCA flow through the multi-path trajectories could be simulated as the flow through porous media [15]. Phantoms mimicking porous media with tunable pore size were thus designed to simulate different MVD and vessel diameter. DCE-US was performed to record the UCA flow through the proposed phantoms, and the velocity and dispersion coefficient were estimated by a model-based deconvolution method. The estimated parameters in different phantoms were then compared to analyze the relationship between microvascular structure and UCA dynamics.

II. METHODS

A. Experimental set-up and data acquisition

An in-vitro experimental set-up consists of a perfusion pump, UCA injector, porous media phantom and the ultrasound acquisition system, which is schematically shown in Fig. 1. In this set-up, the self-designed perfusion pump provided a constant water flow at a rate of 0.22 mL/s. A long tube connected between the pump and the phantom was employed to keep a steady flow. The UCA injector was also connected to the tube by a three-way tap. The porous media phantoms were built by packing alginate beads in a polyurethane tube, whose shape was fixed by two circular nets at two sides of the phantoms. The phantoms were gently squeezed and shaken after packing to provide a more homogeneous structure. The length of the phantoms was comparable to the length of the ultrasound transducer. Variable MVD and vessel diameter were realized by packing beads with diameters of 3.1, 2.5 and 1.6 mm, respectively. In our experiment, the phantoms were submerged in water for ultrasound imaging, avoiding air interference. A 1-mL SonoVue[®] bolus (Bracco, Milan, Italy) at dilution of 1:100 was injected into the flow. DCE-US imaging was performed after the injection using a Verasonics

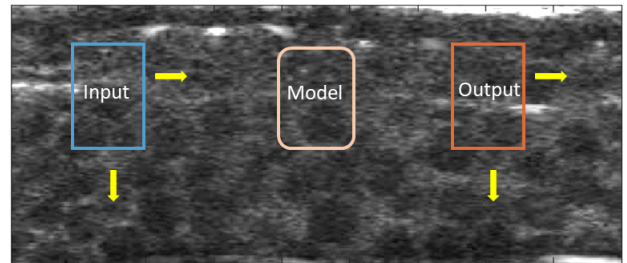


Fig. 2. Model-based input-output analysis.

ultrasound system (Vantage 128, Verasonics Inc.) equipped with a L11-4v probe in contrast mode at a frame rate of 25 Hz for two minutes.

B. Model-based deconvolution

Considering the microvasculature network as a dynamic system, the impulse response of the system could be identified by input-output analysis of TICs. In this experiment, the fluid containing UCA was forced to flow through the porous media phantoms; the UCA transport in the media can thus be described by a convective dispersion process [16]. Accordingly, the differential model that we adopt to describe the kinetics of UCA is the one-dimensional convective-dispersion equation:

$$\partial_t C(z, t) = D \partial_z^2 C(z, t) - v \partial_z C(z, t), \quad (1)$$

where $C(z, t)$ is the concentration of UCA at position z and time t , D is the apparent dispersion coefficient and v is the convective velocity. Moreover, the Green's function of the convective-dispersion equation could be derived as [12, 17],

$$G(z, t | v, D) = \frac{H(t)}{\sqrt{4\pi Dt}} \exp\left(-\frac{(z - vt)^2}{4Dt}\right), \quad (2)$$

where $H(t)$ is the Heaviside function.

As shown in Fig. 2, the UCA bolus flows through the phantom from its left side to its right side, representing the input and output region of interests (ROIs). TICs extracted

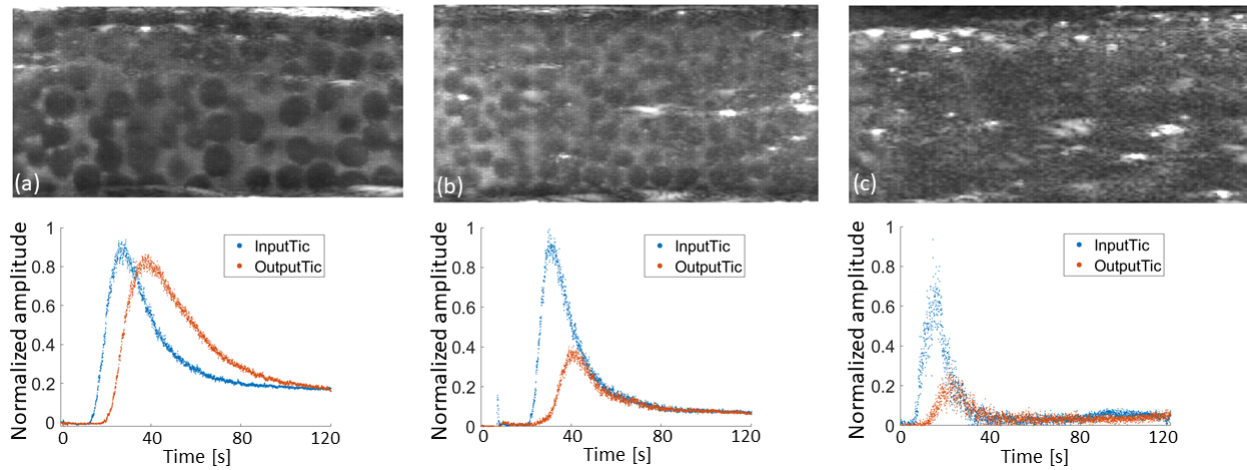


Fig. 3. The maximum intensity persistence images of three porous media phantoms and their corresponding TICs from input and output ROIs: (a) bead size of 3.1 mm, (b) bead size of 2.5 mm, (c) bead size of 1.6 mm.

from input and output ROIs were firstly linearized by taking the square of the intensities. Theoretically, the linearized output matches the convolution of the linearized input with the impulse function of the system in between. By minimizing the mean squared error between the linearized output and the convolution of the linearized input with the Green’s function model, we were able to estimate the convective velocity, v , and dispersion coefficient, D . To reduce the influence of ROI placement, the estimation was repeated 400 times for each phantom by translating the input-output ROIs axially and laterally, and changing the distance between them.

III. RESULTS

Figure 3 shows maximum intensity persistence (MIP) images of three porous media phantoms obtained from their DCE-US acquisitions. With decreasing bead size, the MVD increases and the vessel diameter decreases. Input and output TICs corresponding to three cases are shown in Fig. 3 as well. Qualitatively, with the MVD increasing and vessel diameter decreasing, the TICs become less skewed. Quantitatively, the estimated velocity and dispersion coefficient are shown in Table I.

TABLE I
ESTIMATED VELOCITY AND DISPERSION COEFFICIENT

Bead size	3.1 mm	2.5 mm	1.6 mm
v [mm/s]	3.02 ± 0.19	4.3 ± 0.27	8.3 ± 1.9
D [mm ² /s]	0.02 ± 0.003	0.01 ± 0.0025	0.005 ± 0.0027

IV. CONCLUSION AND DISCUSSION

In this work, an in-vitro experimental set-up is proposed for mimicking microvasculature networks with variable MVD and vessel diameter, and quantitative analysis of the UCA flow through these tissue-mimicking phantoms is presented.

In general, we can conclude that with higher MVD and smaller vessel diameter, obtained by decreasing the bead size, the velocity (v) increases and the dispersion coefficient (D) decreases. These results are in line with our previous in-vivo findings in prostate cancer patients, showing that UCA flow in tumor vasculature is characterized by higher velocity and lower dispersion compared to benign tissue [11, 12]. This investigation evidences a first step in understanding the relationship between microvascular structure and UCA dynamics.

In this experiment, we developed three porous media phantoms with bead size varying from 3.1 mm to 1.6 mm. Looking at the relationship between the estimated parameters and the bead size, a quadratic increasing trend can be identified for the velocity, while a quadratic decreasing trend is observed for the dispersion coefficient. This may reflect the three-dimensional nature of dispersion and the spatial distribution of the beads. Further research is required to confirm and clarify these aspects.

In this work, porous phantoms were obtained by packing beads of the same size. Considering the scenario of tumor-driven angiogenesis, which induces the formation of a microvascular network with vessels of different diameters, phantom constructed by using multiple bead size might be more realistic. This will be pursued in the future to provide a better understanding on how the underlying microvascular structure influences UCA dynamics.

There are several limitations in this work. The UCA flow through phantoms is intrinsically a three-dimensional process, but the DCE-US imaging and subsequent quantitative analysis were performed in 2D. As such, the observed UCA dynamics represent the projection of 3D dynamics onto the imaging plane. Out-of-plane dynamics are therefore lost. Moreover, in this set-up, constant flow was provided by a perfusion pump to mimic the flow in the microvascular network. Although the flow speed is in the order of that expected in the microcirculation (about 2 - 3 mm/s) [18], the resistance of the phantom

may cause UCA bubble disruption when a constant flow is provided, especially in the phantom with small beads. This may influence the result of input-output TICs analysis.

In addition, in a real microvascular network, blood flow moves only within the vessel lumen. However, in the proposed phantoms, flow moves not only in each porous channel but also in the gap between the packed beads and the inner surface of the polyurethane tube. The flow moving in the gap is called superficial flow, which might have different dynamic features compared to flow through porous channels. Moreover, although the developed phantoms represent a useful proof-of-concept for quantitative analysis of UCA dynamics, they cannot fully represent the complex fluid dynamics of UCA in angiogenic vasculature.

To conclude, in this work, we developed dedicated microvascular phantoms and investigated the relationship between UCA dynamics and the underlying microvascular structure. The obtained results are in line with previous in-vivo finding [11, 12], confirming the promise of contrast-ultrasound dispersion imaging for quantification of cancer angiogenesis. In the future, further validation will be performed both in-silico, by dedicated simulations of bubble flow through porous media, and in-vitro, by developing more complex phantoms using beads of polydispersed size.

ACKNOWLEDGMENT

This work is part of the research project LOCATE with project number of 15282, which supported by the Netherlands Organisation for Scientific Research (NWO).

REFERENCES

- [1] F. Bray, J. Ferlay, I. Soerjomataram, R. L. Siegel, L. A. Torre and A. Jemal, "Global Cancer Statistics 2018: GLOBOCAN estimates of incidence and mortality worldwide for 36 cancers in 185 countries," *CA: A Cancer Journal for Clinicians*, vol. 68, pp. 394-424, 2018.
- [2] A. Sidana, M. J. Watson, A. K. George, A. R. Rastinehad, S. Vourganti, S. Rais-Bahrami, A. Muthigi, M. Maruf, J. B. Gordetsky, J. W. Nix, M. J. Merino, B. Turkbey, P. L. Choyke, B. J. Wood, P. A. Pinto, "Fusion prostate biopsy outperforms 12-core systematic prostate biopsy in patients with prior negative systematic biopsy: a multi-institutional analysis," *Urology Oncology*, 341.e1 - e7, 2018.
- [3] F. Bladou, C. Fogaing, M. Levental, S. Aronson, M. Alameldin, M. Anidjar, "Transrectal ultrasound-guided biopsy for prostate cancer detection: Systematic and/or magnetic-resonance imaging-targeted," *Can Urol Assoc J.*, 11: 330-337, 2017.
- [4] J. Folkman, K. Watson, D. Ingber, and D. Hanahan, "Induction of angiogenesis during the transition from hyperplasia to neoplasia," *Nature*, vol. 339, pp. 58-61, 1989.
- [5] M. K. Brawer, "Quantitative microvessel density: a staging and prognostic marker for human prostatic carcinoma," *Cancer*, vol. 78, pp. 345-349, 1996.
- [6] R. J. Eckersley, J. P. Sedelaar, M. J. K. Blomley, H. Wijkstra, N. M. deSouza, D. O. Cosgrove, and J. JMCH de la Rosette, "Quantitative microbubble enhanced transrectal ultrasound as a tool for monitoring hormonal treatment of prostate carcinoma," *The Prostate*, vol. 51, pp. 256-267, 2002.
- [7] N. Elie, A. Kaliski, P. Péronneau, P. Opolon, A. Roche, and N. Lassau, "Methodology for quantifying interactions between perfusion evaluated by DCE-US and hypoxia throughout tumor growth," *Ultrasound Med. Biol.*, vol. 33, pp. 549-560, 2007.
- [8] C. Strouthos, M. Lampaskis, V. Sboros, A. McNeilly, and M. Averkiou, "Indicator dilution models for the quantification of microvascular blood flow with bolus administration of ultrasound contrast agents," *IEEE Transactions on ultrasonics, ferroelectrics, and frequency control*, vol. 57, pp. 1296-1310, 2010.
- [9] D. Cosgrove, "Angiogenesis imaging - ultrasound," *Br. J. Radiol.*, vol. 76, pp. S43 - S49, 2003.
- [10] S. Delorme and M. V. Knopp, "Non-invasive vascular imaging: assessing tumor vascularity," *Eur. Radiol.*, vol. 8, pp. 517 - 527, 1998.
- [11] M. P. J. Kuenen, M. Mischi, and H. Wijkstra, "Contrast-enhanced diffusion imaging for localization of prostate cancer," *IEEE Transactions on Medical Imaging*, vol. 30, pp. 1496 - 1502, 2011.
- [12] R. J. G. van Sloun, L. Demi, A. W. Postema, J. JMCH de la Rosette, H. Wijkstra, M. Mischi, "Ultrasound-contrast-agent dispersion and velocity imaging for prostate cancer localization," *Medical Image Analysis*, vol. 35, pp. 610 - 619, 2016.
- [13] M. P. J. Kuenen, T. A. Saidov, H. Wijkstra, and M. Mischi, "Contrast-ultrasound dispersion imaging for prostate cancer localization by improved spatiotemporal similarity analysis," *Ultrasound Med. Biol.*, vol. 39, pp. 1631-1641, 2013.
- [14] M. P. J. Kuenen, T. A. Saidov, H. Wijkstra, J. JMCH de la Rosette, and M. Mischi, "Correspondence-spatiotemporal correlation of ultrasound contrast agent dilution curves for angiogenesis localization by dispersion imaging," *IEEE Transactions on ultrasonics, ferroelectrics, and frequency control*, vol. 60, pp. 2665-2669, 2013.
- [15] S. Whitaker "Diffusion and dispersion in porous media, *AICHE Journal*, vol. 13, pp. 420 - 427, 1967.
- [16] Z. Qin, R. Fox, S. Subramaniam, R. Pletcher, L. Zhang, "On the apparent particle dispersion in granular media," *Advanced Powder Technology*, vol. 22, pp. 728 - 734, 2011.
- [17] D. G. Duffy, "Green's functions with applications," CRC Press, 2001.
- [18] S. Wojtkiewicz, E. Wojcik-Sosnowska, M. Jasik, R. Maniewski, W. Karnafel, and A. Liebert, "Assessment of speed distribution of red blood cells in the microvascular network in healthy volunteers and type 1 diabetes using laser Doppler spectra decomposition," *Physiological Measurement*, vol. 35, pp. 283-295, 2014.